Power Optimization of Wireless Media Systems with Space-Time Code Building Blocks

Homayoun Yousefi’zadeh Hamid Jafarkhani Mehran Moshfeghi

Department of Electrical Engineering and Computer Science

University of California, Irvine

[hyousefi,hamidj,mmoshfeg]@uci.edu

Abstract

We present an analytical solution to the problem of power control in wireless media systems with multiple transmit antennas. We formulate an optimization problem aimed at minimizing total power consumption of wireless media systems subject to a given level of Quality of Service (QoS) and an available bit rate. Our formulation takes into consideration the power consumption related to source coding, channel coding, and transmission of multiple transmit antennas. In our study, we consider Gauss-Markov and video source models, Rayleigh fading channels along with the Bernoulli/Gilbert-Elliott loss models, and space-time transmission block codes.

Index Terms

Wireless Media Systems, Power Optimization, Source Coding, Channel Coding, Multiple Transmit Antenna Systems, Space-Time Block Codes, Bernoulli Loss Model, Gilbert-Elliott Loss Model, QoS, Rate, Distortion.

I. Introduction

The emergence of new wireless standards is expected to expedite the delivery of the next generation high quality portable multimedia systems. More frequent and longer use of portable multimedia systems is naturally equivalent to higher power consumption of mobile devices. This requires that the power consumption of such devices be kept to a minimum level in order to extend the lifetime of their limited power resources. On the contrary, providing the desired level of quality of service in the presence of the fading effects of multipath wireless channels necessitates higher consumption of power in mobile devices. The theme representing the goal of this paper is, hence, to address the tradeoff between the power consumption and the quality of service in wireless media systems. Fig. 1 includes an illustration of the general model of a communication system utilized to transmit multimedia content across a wireless backbone. We note that the model utilizes a multiple transmit antenna system. Generally speaking, optimizing power for transmitting and receiving multimedia content to and from a mobile host requires addressing

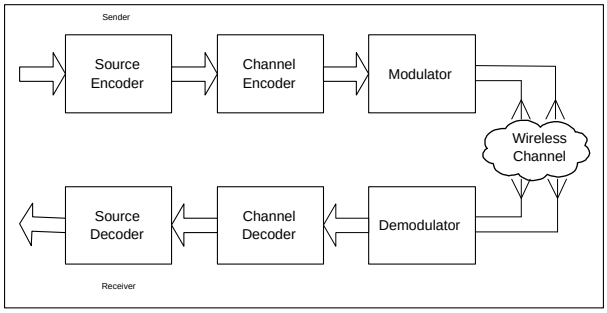

Fig. 1. An illustration of the multiple antenna communication system.

the power consumption tradeoff among different components of the communication system. The latter is of special importance considering the quality of service issues as well as time-varying characteristics of the underlying wireless channel. The power consumed in a mobile device is for the most part associated with source coding, channel coding, and transmission. The processing power of source coding and channel coding is typically a function of the underlying utilized algorithms. The transmission power depends on the bit rate and the unit transmission power. While reducing transmission power leads to longer life time of the power resources of a mobile device and lower interference with the transmission of the other mobile devices, it increases the error rate of the mobile device itself.

In what follows we briefly review some of the specific literature articles in the context of transmitting multimedia content across a wireless backbone. In an early work, Lan et al. [13] solved an energy optimization problem subject to quality of service constraints for transmitting images across the wireless backbone. However, they did not consider the time-varying characteristics of the wireless channel in the analysis of channel coding and transmission. Goel et al. [8] solved another image transmission energy optimization problem subject to distortion and rate constraints. While they appropriately considered hardware specific impacts in their work, their analysis lacked a consideration of channel coding and transmission with respect to the time-varying characteristics of the wireless channel. Havinga [9] considered energy efficiency in channel coding techniques for wireless systems without considering the

energy of source coding and transmission. Stuhlmuller et al. [18] derived a rate-distortion model for an H.263 compliant coder based on simulation data. Their model could also be used for other codecs that rely on hybrid motion compensation. Appadwedula et al. [5] formulated an energy optimization problem subject to statistical distortion and rate constraints for transmitting images over wireless channels. Considering transmission, source, and channel coding components in the formulation of the problem, the authors deployed a gradient based method to solve the problem. Without considering transmission power, Zhang et al. [11] proposed a generic power optimization problem subject to distortion and rate constraints for transmitting video across wireless backbone. The formulation of the latter problem considered the time-varying characteristics of memoryless wireless channels relying on joint source-channel coding employing Unequal Error Protection (UEP) techniques. The authors solved the problem relying on iterative gradient-based techniques. As proposed in [12], Ji and the same group of authors extended the results of their previous work to consider power consumption due to transmission in wireless systems. The analysis of [12] utilized a high level motion estimation technique that could well fit into H.263 or MPEG-2 source coding standards, an Unequal Error Protection (UEP) technique based on the Bernoulli loss model in conjunction with the Reed-Solomon channel coding, and a single transmit antenna system. Focusing on uplink mobile-to-base-station scenarios, Lu et al. [14] solved a similar power optimization problem subject to the end-to-end distortion of [18] relying on the H.263 source coding scheme and Reed-Solomon channel coding in conjunction with the Gilbert loss model. We point out that none of the literature articles cited above have provided an analytical solution along with an analysis of complexity to their formulated optimization problem or considered wireless systems deploying multiple transmit antennas. Considering the real-time nature of the problem, we argue that providing an analytical solution to a power optimization problem for wireless systems is attractive as it can potentially offer lower space and time complexity solutions. In addition, the use of multiple transmit antenna systems in wireless systems as proposed by WCDMA and CDMA2000 standards is gaining an ever increasing popularity.

The main contribution of this paper is in the following areas. First, the paper proposes the use of multiple transmit antenna systems with space-time block codes instead of traditional single antenna systems. Second, the paper considers three different channel loss models, namely Bernoulli, Gilbert, and Gilbert-Elliott models, to properly capture the loss behavior of different transmission channels. While the paper relies on closed form expressions of the loss model in the first two cases as proposed in [20], it utilizes a recursive expression to describe the behavior of the last loss model. Third relying on the analysis of multiple transmit antenna systems along with various channel loss models, the paper formulates a set of power optimization problems aimed at minimizing the combined power of source coding, channel coding, and transmission while considering rate and distortion constraints. The paper provides analytical solutions to the optimization problems utilizing Bernoulli and Gilbert loss models and an iterative solution to the optimization problem using the Gilbert-Elliott loss model.

An outline of the paper follows. In Section II, we provide an analysis of the transmission and the channel coding components of the underlying wireless system. In this section, we express the symbol error rate as a function of the average received signal to noise ratio. Next relying on the Bernoulli and Gilbert-Elliott loss models, we express the residual symbol error rate as a function of the underlying loss model of the system and the symbol error rate. In Section III, we provide an analysis of the source coding and distortion for the underlying wireless system. Starting from a simple Gauss-Markov source model, we generalize our analysis to a video source and obtain associated overall distortions for each case. In Section IV, we formulate and solve our power optimization problem subject to distortion and rate constraints. In Section V, we numerically validate our analytical results. Finally, Section VI includes a discussion of concluding remarks and future work.

II. Transmission and Channel Coding Analysis

We start our discussion by providing an analysis of the underlying transmission system and the wireless fading channel.

A. Transmission and Fading Channel Analysis

First, we focus on the analysis of the wireless fading channel. We rely on the so-called Rayleigh model with a fading factor α to describe the wireless channel. We note that the output signal of such a channel S_o can be related to its input signal S_i as

$$S_o = \alpha\, S_i \; + \; N \tag{1}$$

where N indicates the noise signal. Further, we recall that for a multipath slow fading Rayleigh wireless channel, the average received signal to noise ratio is expressed as

$$\overline{SNR} = \mathcal{E}[|\alpha|^2]\, \frac{E_{sym}}{N_0} \tag{2}$$

where $\overline{SNR}$ represents the average received signal to noise ratio of the demodulator of Fig. 1, $\mathcal{E}$ denotes the expectation operator, $|\alpha|$ has a Rayleigh distribution, E_{sym} is the transmission symbol energy, and N_0 is the one-sided spectral density of the white Gaussian noise. Simon et al. [16] showed that the symbol error rate of a single transmit, single receive antenna system for a slow fading Rayleigh channel utilizing L-PSK modulation scheme is expressed as

$$\begin{aligned} e_{sym} = \quad & \tfrac{L-1}{L}\,\{1 - \sqrt{\tfrac{A\,\overline{SNR}}{1+A\,\overline{SNR}}}\,\tfrac{L}{(L-1)\pi} \\ & \times [\tfrac{\pi}{2} + \arctan(\sqrt{\tfrac{A\,\overline{SNR}}{1+A\,\overline{SNR}}}\cot\tfrac{\pi}{L})]\} \end{aligned} \tag{3}$$

where $A = \overline{SNR}\,\sin^2(\frac{\pi}{L})$ and the number of bits per symbol m is related to the number of signal points in the constellation L as $m = \log_2 L$. The result of Equation (3) for BPSK modulation scheme where $m = 1$ and $L = 2$ is expressed as

$$e_{sym} = \frac{1}{2}\,\{1 - \sqrt{\frac{\overline{SNR}}{1+\overline{SNR}}}\} \tag{4}$$

Similarly, the result for the QPSK modulation scheme where $m = 2$ and $L = 4$ is expressed as

$$e_{sym} = \frac{3}{4}\{1 - \frac{4}{3\pi}\sqrt{\frac{\overline{SNR}}{2+\overline{SNR}}}[\frac{\pi}{2} + \arctan\sqrt{\frac{\overline{SNR}}{2+\overline{SNR}}}]\} \tag{5}$$

Further, Simon [17] introduced closed forms for the slow fading Rayleigh channel symbol error rate of a two transmit, M receive antenna system utilizing the space-time block codes of [1] and [19]. He showed the symbol error rate for the L-PSK modulation scheme is expressed as

$$e_{sym} = \frac{1}{2}\{1 - \sqrt{\frac{2A}{1+2A}}\sum_{k=0}^{2M-1}\binom{2k}{k}[\frac{1}{4(1+2A)}]^k\} \tag{6}$$

where $A = \overline{SNR}\sin^2(\frac{\pi}{L})$. We note that for a single receive antenna where $M = 1$, the result of Equation (6) for the BPSK modulation scheme is expressed as

$$e_{sym} = \frac{1}{2}\{1 - \sqrt{\frac{2\,\overline{SNR}}{1+2\,\overline{SNR}}}[1 + \frac{1}{2(1+2\,\overline{SNR})}]\} \tag{7}$$

Similarly for a single receive antenna where $M = 1$, the result for the QPSK modulation scheme is expressed as

$$e_{sym} = \frac{1}{2}\{1 - \sqrt{\frac{\overline{SNR}}{1+\overline{SNR}}}[1 + \frac{1}{2(1+\overline{SNR})}]\} \tag{8}$$

B. Loss and Channel Coder Analysis

Having specified the symbol error rate based on the channel characteristics, we propose utilizing a Reed-Solomon channel coder $RS(n,k)$ that converts k information symbols into an n-symbol block as the result of appending $(n-k)$ parity symbols. Assuming R_s and R_c respectively denote source and channel coding bit rates, we note that utilizing such a channel coding scheme introduces a channel code rate $r = \frac{k}{n} = \frac{R_s}{R_s+R_c}$. The scheme also allows for correcting $t_c = \lfloor\frac{n-k}{2}\rfloor$ symbol errors. In order to calculate the error rate of a block utilizing an $RS(n,k)$ coder, we consider the single-state Bernoulli, the two-state Gilbert [7], and the generalized two-state Gilbert-Elliott [4] error models. We note that while the first model represents a memoryless channel, the other two represent channels with memory.

The single state Bernoulli model is the simplest model describing symbol loss in a memoryless channel. In the Bernoulli model, one assumes that the probabilities of loss among different symbols are temporally independent. Noting the fact that losing more than t_c symbols from n transmitted symbols results in a block loss, the probability of block loss, also known as the residual symbol error rate, for the Bernoulli model is given by

$$\Psi(n, t_c) = \sum_{i=t_c+1}^{n} \binom{n}{i} e_{sym}^{i} (1 - e_{sym})^{(n-i)} \tag{9}$$

where e_{sym} is the symbol error rate.

As pointed out in many research articles, a multipath fading wireless channel typically undergoes burst loss representing temporally correlated loss. The two-state Gilbert-Elliott loss model provides an elegant mathematical model to capture the loss behavior of ever-changing channel conditions. In the Gilbert-Elliott model, symbol loss is described by a two-state Markov chain as described in Fig. 2. The first state G known as the GOOD state represents the loss of a symbol with probability e_G while the other state B known as the BAD state represents the loss of a symbol with probability e_B where $e_B >> e_G$. The GOOD state also introduces a probability $P_G = \gamma$ of staying in the GOOD state and a probability $1 - P_G$ of transitioning to the BAD state while the BAD state introduces a probability $P_B = \beta$ of staying in the BAD state and a probability $1 - P_B$ of transitioning to the GOOD state. The parameters γ and β can be typically measured from the observed loss rate and burst length. In [20] we study temporally correlated

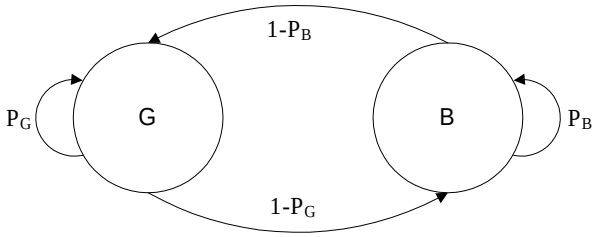

Fig. 2. The two-state Gilbert-Elliott loss model with the state transition probabilities $1 - P_G$ and $1 - P_B$ for $P_G = \gamma$ and $P_B = \beta$. The symbol loss probabilities are specified by e_G and e_B where $e_G << e_B$.

loss behavior of IP packet networks employing the Gilbert loss model. In that article we show that for the Gilbert loss model of [7] with $e_G = 0$ and $e_B = 1$, the closed form expression for the probability of receiving exactly k symbols from n transmitted symbols is given by

$$P(n,k) \;=\; P(n,k,G) + P(n,k,B) \tag{10}$$

The probability of receiving exactly k symbols from n transmitted symbols and winding up in the GOOD state $P(n,k,G)$ is given by

$$\begin{aligned} P(n,k,G) \;=\; & \\ & \gamma^{2k-n}\,(1-\beta)\,(1-\gamma)\,\{ \\ & \quad \textstyle\sum_{i=0}^{n-k-1} \binom{n-k-1}{i}\binom{k}{i+1}(\beta\,\gamma)^{n-k-1-i}\,[(1-\beta)\,(1-\gamma)]^i \\ & \}\,g_{ss} \quad + \quad \gamma^{2k-n-1}\,(1-\beta)\,\{ \\ & \quad \textstyle\sum_{i=0}^{n-k} \binom{n-k}{i}\binom{k-1}{i}(\beta\,\gamma)^{n-k-i}\,[(1-\beta)\,(1-\gamma)]^i \\ & \}\,b_{ss} \end{aligned} \tag{11}$$

for $n \geq k+1$, steady state probability of the GOOD state $g_{ss} \;=\; \frac{1-\beta}{2-\gamma-\beta}$, and steady state probability of the BAD state $b_{ss} \;=\; \frac{1-\gamma}{2-\gamma-\beta}$. Similarly, the probability of receiving exactly k symbols from n transmitted symbols and winding up in the BAD state $P(n,k,B)$ is given by

$$\begin{aligned} P(n,k,B) \;=\; & \\ & \gamma^{2k-n+1}\,(1-\gamma)\,\{ \\ & \quad \textstyle\sum_{i=0}^{n-k-1} \binom{n-k-1}{i}\binom{k}{i}(\beta\,\gamma)^{n-k-1-i}\,[(1-\beta)\,(1-\gamma)]^i \\ & \}\,g_{ss} \quad + \quad \gamma^{2k-n}\,(1-\beta)\,(1-\gamma)\,\{ \\ & \quad \textstyle\sum_{i=0}^{n-k-1} \binom{n-k}{i+1}\binom{k-1}{i}(\beta\,\gamma)^{n-k-1-i}\,[(1-\beta)\,(1-\gamma)]^i \\ & \}\,b_{ss} \end{aligned} \tag{12}$$

for the same description of the parameters. The initial conditions for Equation (11) and Equation (12) are

expressed below.

$$\begin{aligned} P(k,0,G) &= 0 \\ P(k,k,B) &= 0 \\ P(k,k,G) &= \gamma^k\, g_{ss} + (1-\beta)\gamma^{(k-1)}\, b_{ss} \\ P(k,0,B) &= (1-\gamma)\beta^{(k-1)}\, g_{ss} \;+\; \beta^k\, b_{ss} \end{aligned} \tag{13}$$

While our model is of special interest from the stand point of providing an analytical lower-complexity solution to a power optimization problem such as the one proposed in [14], we take a step further in this study by relying on the general Gilbert-Elliott loss model to best describe the loss behavior of a wireless channel. In [10], we provide effective ways of measuring the parameters of the Gilbert-Elliott loss model. For the Gilbert-Elliott loss model, the probability of receiving exactly k symbols from n transmitted symbols is still described by Equation (10). However, the recursive probabilities of receiving exactly k symbols from n transmitted symbols and winding up in the GOOD state and the BAD state are respectively given by

$$\begin{aligned} &P(n,k,G) \;= \\ &\quad e_G\,[\gamma\, P(n-1,k,G) \;+\; (1-\beta)P(n-1,k,B)] \\ &\quad (1-e_G)\,[\gamma\, P(n-1,k-1,G) \\ &\qquad\qquad + (1-\beta)P(n-1,k-1,B)] \end{aligned} \tag{14}$$

and

$$\begin{aligned} &P(n,k,B) \;= \\ &\quad e_B\,[(1-\gamma)\, P(n-1,k,G) \;+\; \beta P(n-1,k,B)] \\ &\quad (1-e_B)\,[(1-\gamma)\, P(n-1,k-1,G) \\ &\qquad\qquad + \beta P(n-1,k-1,B)] \end{aligned} \tag{15}$$

for $n \geq k > 0$ and the initial conditions

$$\begin{aligned} P(0,0,G) &= g_{ss} = \tfrac{1-\beta}{2-\gamma-\beta} \\ P(0,0,B) &= b_{ss} = \tfrac{1-\gamma}{2-\gamma-\beta} \\ P(1,0,G) &= e_G\,[\gamma\, g_{ss} + (1-\beta)\, b_{ss}] \\ P(1,0,B) &= e_B\,[(1-\gamma)\, g_{ss} + \beta\, b_{ss}] \end{aligned} \tag{16}$$

Utilizing Equation (10) along with Equation (14) and Equation (15) for the Gilbert-Elliott model, the residual symbol error rate or the probability of a block loss is given by

$$\Psi(n, t_c) = 1 - \sum_{k=n-t_c}^{n} P(n,k) \tag{17}$$

It is also important to note that utilizing the two-state Gilbert-Elliott model calls for changing Equation (2) in order to distinguish between the symbol error rates of the GOOD state and the BAD state. Assuming $N_{0,G}$ denotes the one-sided spectral density of the white Gaussian noise in the GOOD state, the average received signal to noise ratio of the GOOD state is expressed as

$$\overline{SNR_G} = \mathcal{E}[|\alpha|^2]\, \frac{E_{sym}}{N_{0,G}} \tag{18}$$

Similarly assuming $N_{0,B}$ denotes the one-sided spectral density of the white Gaussian noise in the BAD state, the average received signal to noise ratio of the BAD state is expressed as

$$\overline{SNR_B} = \mathcal{E}[|\alpha|^2]\, \frac{E_{sym}}{N_{0,B}} \tag{19}$$

where $N_{0,G} << N_{0,B}$ and the other parameters are the same as in Equation (2).

III. Source Coding and Distortion Analysis

In this section, we focus on the source coding and the distortion analysis. In order to validate our model, we first provide an analysis of distortion utilizing a Gauss-Markov source model and then continue with an experimental video source model.

A. Analysis of Distortion based on the Gauss-Markov Source Model

In this subsection, we provide an analysis of the distortion utilizing the so-called Gauss-Markov model. We note that the analysis of this section is provided as a proof of concept. In the next section, we provide an analysis for a more realistic model utilizing an experimental H.263 video source coding model.

For the source coding analysis of this section, we utilize a first order Gauss-Markov source with a variance σ_{gm}^2 and a correlation coefficient ρ. As described in [6], utilizing such a model for a transform coder introduces an operational distortion-rate function in the form of

$$D_{tc}(R_s) = \xi\, \sigma_{gm}^2\, (1-\rho^2)^{\frac{k-1}{k}}\, 2^{-2R_s} \tag{20}$$

where ξ is a constant depending on the quantizer utilized for the transform coefficients, k and R_s are defined in the previous section. We note that the Gauss-Markov model of Equation (20) is reduced to a pure Gaussian source model by setting $\xi = 0$. In our model, any symbol associated with an unrecovered block is replaced by the Gaussian mean, thereby introducing a distortion of σ_{gm}^2. Consequently, the overall distortion at the decoder is calculated by taking the average of block recovery and block loss distortions multiplied by their associated probabilities. Assuming a block loss probability of $\Psi(n, t_c)$, the overall distortion D_{total} is calculated as

$$\begin{aligned} D_{total} &= D_s + D_v \\ &= (1 - \Psi(n, t_c))\, D_{tc} + \Psi(n, t_c)\, \sigma_{gm}^2 \end{aligned} \tag{21}$$

Again, we note that the block loss probability is the same as the residual symbol error rate and can be calculated from Equation (9) in the case of utilizing the Bernoulli loss model and from Equation (17) in the case of utilizing the Gilbert or the Gilbert-Elliott loss models.

B. Analysis of Distortion based on An Experimental H.263 Video Source Model

In this subsection, we provide an analysis of distortion utilizing a more realistic H.263 compliant source coder. For the source coding analysis of this section, we rely on the experimental results of Stuhlmuller et

al. [18]. The experimental distortion model of [18] consists of two components D_s and D_v respectively imposed by the source encoder and the video decoder. The model relies on an INTRA update scheme forcing a macroblock (MB) to be coded in the INTRA-mode after every $T-1$ macroblocks and resulting in a source encoder distortion of

$$D_s(\omega, R_s) = \frac{\theta(\omega)}{R_s - R_I(\omega)} + D_I(\omega) \tag{22}$$

where $\omega = \frac{1}{T}$ is the INTRA rate, R_s is the encoding bit rate in $kbps$ and D_s is the distortion in terms of the mean square error per source sample. The measurements of [18] also suggest that the distortion-rate parameters θ, R_0, and D_0 depend linearly on the percentage of INTRA coded macro blocks ω as shown by the following equations.

$$\begin{aligned} \theta &= \theta_P + \Delta\theta_P\,\omega \\ R_I &= R_{IP} + \Delta R_{IP}\,\omega \\ D_I &= D_{IP} + \Delta D_{IP}\,\omega \end{aligned} \tag{23}$$

The model parameters θ_P, $\Delta\theta_P$, R_{IP}, ΔR_{IP}, D_{IP}, and ΔD_{IP} characterize the coding of the input video sequence with the given motion compensated H.263 encoder in baseline mode. It is important to note that the parameters highly depend on the spatial detail and the amount of motion in the sequence.

Reference [18] also proposes that the video coder distortion caused by transmission errors is expressed as

$$D_v(\omega, \Psi) = \sigma_{u0}^2\,\Psi(n, t_c) \sum_{t=0}^{T-1} \frac{1-\omega t}{1+\lambda t} \tag{24}$$

where leakage λ describes the efficiency of loop filtering to remove the error and σ_{u0}^2 describes the sensitivity of the video decoder to an increase in error rate. In addition, the residual symbol error rate $\Psi(n, t_c)$ can be calculated as described in the previous section. The overall distortion D_{total} at the video decoder is then calculated as

$$D_{total} = D_s + D_v \tag{25}$$

IV. Power Optimization

In this section, we focus on power optimization of a mobile device utilized in a wireless media system with space-time code building blocks. Recalling that the overall power consumed in a mobile device is associated with source coding, channel coding, and transmission, we first introduce individual terms expressing the consumed power of different components. We then proceed with the formulation of the power optimization problem and the solution to it.

A. Power Optimization Formulation

The first power consumption component of the underlying wireless system is the source encoder. We consider the power consumption of the source encoder in the case of utilizing both the Gauss-Markov source of Section III.A and the video source of Section III.B.

We start by considering the power consumption of the Gauss-Markov source encoder of Section III.A. Considering the fact that the encoder rate is the dominant factor of the power consumption of a Gauss-Markov source encoder, we express the power consumption of such a source encoder as a linear function of the encoder rate, i.e.,

$$P_s(R_s) \;=\; \epsilon_s\,(a_{ls} \;+\; c_{ls}R_s) \tag{26}$$

where a_{ls} and c_{ls} are the linear model constants.

Next, we consider the power consumption of the video source encoder of Section III.B. Reference [14] proposes the following average power consumption model for an H.263 coder

$$\begin{aligned} P_s(\omega, R_s) \;=\; & \tfrac{\epsilon_s f_r N_{MB}}{T}[(E_{DCT} \;+\; E_Q) \\ & + (T-1)(E_{DCT} \;+\; E_Q \;+\; E_{ME})] \end{aligned} \tag{27}$$

where ϵ_s is the weighting factor introduced to allow for the scaling of the model based on the actual power consumption of a particular implementation, f_r is the frame rate, N_{MB} is the number of macroblocks in a

frame, and T is described in Section III.B. Further E_{DCT}, E_Q, and E_{ME} respectively denote the energy consumed by DCT, quantization [1], and motion estimation. Assuming

$$\begin{aligned} a_s &= f_r N_{MB}(E_{DCT} + E_{ME}) \\ b_s &= f_r N_{MB} E_{ME} \\ c_s &= f_r N_{MB} \frac{E_Q}{R_s} \end{aligned} \tag{28}$$

Equation (27) can be expressed as

$$P_s(\omega, R_s) = \epsilon_s (a_s - b_s \omega + c_s R_s) \tag{29}$$

where a_s, b_s, c_s are described in terms of the energy consumptions of different source coding components, ω is again the source coder INTRA rate, and R_s again indicates the source coding bit rate. The authors of [14] confirm that the measured power consumptions for encoding the sequences Containership.qcif, Foreman.qcif, MotherDaughter.qcif, News.qcif, and SilentVoice.qcif with an H.263 software encoder fit the model parameters of Equation (29) quite accurately. We note that Equation (29) can be reduced to Equation (26) in the case of utilizing a Gauss-Markov source model verifying the consistency of the two models. The latter is justified considering the lack of any motion estimation power in the consumed power of the Gauss-Markov source model resulting in coding all of the macro blocks of Section III.B in INTRA-mode, i.e., $\omega = 1$.

The second power consumption component of the underlying wireless system is the channel coder. Reference [5] models per bit energy consumption of a Reed-Solomon $RS(n, k)$ encoder as

$$P_c(R_s, R_c) = \epsilon_c \frac{n R_s R_c}{m(R_s + R_c)} \tag{30}$$

where ϵ_c is a scaling factor and m is the number of bits per symbol.

Finally, the third power consumption component of the underlying wireless system is the transmitter.

[1] Quantization energy also includes the energy consumed by variable length coding (VLC).

The total transmission power is given by

$$P_t(R_s, R_c, E_{sym}) \;=\; \epsilon_t \, E_{sym}(R_s + R_c) \tag{31}$$

where ϵ_t is a scaling factor that maps the radiated energy into the actual transmission power of a wireless device.

Having expressed all of the power consumption components as well as the distortion terms, we now formulate our power optimization problem subject to distortion and rate constraints as

$$\min_{\omega, R_s, R_c, E_{sym}} \; P_{total} \;=\; P_s + P_c + P_t \tag{32}$$

$$\text{Subject To:} \quad D_{total} \;=\; D_s \;+\; D_v \;\leq\; D_0 \tag{33}$$

$$R_{total} \;=\; R_s \;+\; R_c \;\leq\; R_0 \tag{34}$$

In the rest of this section, we utilize the more general video source model of Section III.B, making note of the fact that the model of Equation (29) can be reduced to that of Equation (26) by setting $\omega = 1$ and considering $a_{ls} = a_s - b_s$ and $c_{ls} = c_s$. We observe that for a single/multiple transmit antenna wireless system utilizing the L-PSK modulation scheme, the objective function and inequality constraints of the above optimization problem can be expressed in terms of optimization variables ω, R_s, R_c, and E_{sym} as well as some constants. The following set of equations illustrate the matter in the case of utilizing the QPSK modulation scheme along with the more general source encoder model of Section III.B. First note that the total power is expressed as

$$\begin{aligned} P_{total} \;=\; & \epsilon_s(a_s \;-\; b_s\omega \;+\; c_s R_s) \;+ \\ & \epsilon_c \tfrac{n R_s R_c}{m(R_s + R_c)} \;+\; \epsilon_t \tfrac{E_{sym}}{m}(R_s + R_c) \end{aligned} \tag{35}$$

Next, note that the distortion terms are expressed as

$$\begin{aligned} D_s &= \frac{\theta_P + \Delta\theta_P\,\omega}{R_s - (R_{0P} + \Delta R_{0P}\,\omega)} + D_{0P} + \Delta D_{0P}\,\omega \\ D_v &= \sigma_{u0}^2 \Psi \sum_{t=0}^{T-1} \frac{1-\omega t}{1+\lambda t} = \\ & \sigma_{u0}^2 \sum_{t=0}^{T-1} \frac{1-\omega t}{1+\lambda t} \sum_{k=t_c+1}^{n} \binom{n}{k} (e_{sym})^k (1-e_{sym})^{n-k} \end{aligned} \tag{36}$$

Finally, note that the symbol error rate term is expressed as

$$e_{sym} = \frac{1}{2}\{1 - \sqrt{\frac{\frac{\mathcal{E}[|\alpha|^2]E_{sym}}{N_0}}{1+\frac{\mathcal{E}[|\alpha|^2]E_{sym}}{N_0}}}[1 + \frac{1}{2(1+\frac{\mathcal{E}[|\alpha|^2]E_{sym}}{N_0})}]\} \tag{37}$$

The derivation of the equations is similar for the L-PSK modulation relying on Equations (29), (30), (31) along with (22), (23), (2), (3), (6), (9), and (24).

B. Power Optimization Solutions

In this section , we provide a discussion of solving the optimization problem formulated by Equation (32) along with the constraint set (33) and (34). Again considering the more general form of Equation (29), we utilize the video source model of Section III.B in the discussion of this section. Further, we consider two scenarios.

In the first scenario, we assume that the cost function and the constraints of the optimization problem can all be expressed in closed forms. This is clearly seen in the case of utilizing the Bernoulli loss model as well as the simplified Gilbert model. Relying on the Lagrangian theory, we convert the problem to an optimization problem without constraints. We define the Lagrangian function of Equation (32) as

$$\begin{aligned} LG_P = P_s + P_c + P_t + \\ \mu_1 (D_s + D_v - D_0) + \mu_2 (R_s + R_c - R_0) \end{aligned} \tag{38}$$

where the parameters μ_1 and μ_2 are the Lagrange multipliers in the Lagrangian Equation (38). The unconstrained minimization problem for $\Omega = \{\omega, R_s, R_c, E_{sym}\}$ is defined as

$$\begin{aligned} \min_\Omega LG_P = \min_\Omega \{P_s + P_c + P_t + \\ \mu_1 (D_s + D_v - D_0) + \mu_2 (R_s + R_c - R_0)\} \end{aligned} \tag{39}$$

Conditions of Optimality: Constraint Qualifications

We now investigate the existence of necessary and sufficient optimality conditions also known as constraint qualifications. For our unconstrained minimization problem

$$\min_{\omega, R_s, R_c, E_{sym}} LG_P \tag{40}$$

the constraint qualifications are expressed in terms of Lagrange multiplier theory [2]. They revolve around conditions under which Lagrange multiplier vectors satisfying the following conditions are guaranteed to exist for a local minimum $\Omega^* = \{\omega^*, R_s^*, R_c^*, E_{sym}^*\}$. The local minimum satisfies

$$\nabla LG_P(\Omega^*) = 0 \tag{41}$$

where $\nabla LG_P = [\frac{\partial LG_P}{\partial \omega}, \frac{\partial LG_P}{\partial R_s}, \frac{\partial LG_P}{\partial R_c}, \frac{\partial LG_P}{\partial E_{sym}}, \frac{\partial LG_P}{\partial \mu_1}, \frac{\partial LG_P}{\partial \mu_2}]$. Further, $\mu_k^* \geq 0$ for $k = 1, 2$ if associated with an active inequality at Ω^*, i.e.,

$$\begin{cases} \mu_1^* \geq 0 & : \quad if\ D_s + D_v = D_0 \\ \mu_1^* = 0 & : \quad otherwise \end{cases} \tag{42}$$

and

$$\begin{cases} \mu_2^* \geq 0 & : \quad if\ R_s + R_c = R_0 \\ \mu_2^* = 0 & : \quad otherwise \end{cases} \tag{43}$$

Constraint qualifications guarantee the existence of unique Lagrange multipliers for a given local minimum Ω^* if the active inequality constraint gradients of (33) and (34) are linearly independent [3].

We note that the objective function (32) defined over a compact subset of $\mathcal{R}^4$ is continuously differentiable and the constraint gradients of (33) and (34) are linearly independent. Finding the solution to the optimization problem is, therefore, equivalent to finding the solution to the equation set (41) specifying optimization variables ω, R_s, R_c, and E_{sym}.

It is important to observe that the formulated problem of (32) is subject to discrete constraints applied to the source coding variable $\omega = \frac{1}{T}$ and the channel coding variable $r = \frac{k}{n} = \frac{R_s}{R_s + R_c}$. Solving the problem of (32) is hence categorized under discrete constraint optimization problems which can be solved with the following approach. The approach is to add extra discrete constraints effectively changing the formulation of the optimization problem from a NonLinear Programming (NLP) to a Mixed Integer NonLinear Programming (MINLP) in which the variables ω and R_c can only take on discrete values. In this approach, one selects the best solution among the set of solutions to the problems obtained for different discrete values of the optimization parameters [2].

In the second scenario, we consider the cases in which the cost function and/or some of the optimization constraints cannot be expressed in closed forms. This is clearly seen in the case of utilizing the general Gilbert-Elliott loss model in which the video coder distortion constraint of (24) cannot be expressed in a closed form. Considering the fact that constraints (33) and (34) are convex[2] , we propose deploying the Sequential Quadratic Programming (SQP) technique. In SQP the necessary conditions for optimality are represented by the Kuhn-Tucker (KT) equations described by Equation (41) and the conditions below.

$$\begin{aligned} \mu_1^* \left(D_s^* + D_v^* - D_0^*\right) &= 0 \\ \mu_2^* \left(R_s^* + R_c^* - R_0^*\right) &= 0 \\ \mu_1^*,\, \mu_2^* &\geq 0 \end{aligned} \tag{44}$$

A variant of the quasi-Newton method can then be used to iteratively find the solution to the optimization problem [15]. We note that utilizing a variant of the quasi-Newton method is equivalent to solving a quadratic estimation of the problem in every iteration.

We end this section by providing an analysis of the complexity for the two scenarios described above. Taking the discrete constraints into consideration and assuming p represents the number of parameter

[2]The function $f : \mathcal{C} \longmapsto \mathcal{R}^n$ defined over the convex set $\mathcal{C} \subseteq \mathcal{R}^n$ is called convex if $\forall x_1, x_2 \in \mathcal{C}$ and $0 \leq \alpha \leq 1$ the inequality $f(\alpha x_1 + (1-\alpha)x_2) \leq \alpha f(x_1) + (1-\alpha) f(x_2)$ holds.

combinations, the time complexity of solving the problem of (41) for the first scenario is $\mathcal{O}(p\,n\log n)$ where n indicates the degree of (41). The complexity determines the overall complexity of the solution considering the fact that the rest of the calculations are in a lower time complexity order. Similarly, the time complexity of solving the problem of (41) for the second scenario is $\mathcal{O}(I\,p\,n\log n)$ where I indicates the number of iterations and n indicates the degree of the quadratic estimation. We have observed that few iterations are required for convergence in the case of the second scenario. The complexity results are, therefore, quite good compared to other recursive optimization approaches such as dynamic programming introducing a time complexity in the order of $\mathcal{O}(p\,n^2)$.

V. Numerical Analysis

In this section, we numerically validate our analytical results. Before proceeding with the explanation of our numerical results, we note that we are solving the power optimization problem for both single and double transmit antenna wireless systems. In the case of a double transmit antenna system, we assume that two signals are transmitted simultaneously from the two transmit antennas at each time slot. In addition, we assume that the slow fading wireless channel characterized by a Rayleigh distribution is quasi-static and flat implying that the path gains are constant over a frame but vary independently from one frame to another.

When utilizing the Gauss-Markov source of Section III.A, we report our results for $\rho = 0$ and $\rho = 0.9$ respectively indicating a memoryless Gaussian source and a highly correlated source with behavior close to a video source. Our experiments for the H.263 video source encoder of Section III.B span over source coding parameter settings associated with the sequences Containership.qcif, Foreman.qcif, MotherDaughter.qcif, News.qcif, and SilentVoice.qcif. However, we only report the results for Containership.qcif. In addition, we select the scaling factors $[\epsilon_s, \epsilon_c, \epsilon_t]$ as $[1, 0.01, 1]$ and $[10, 0.1, 1]$ respectively simulating transmission systems that implement hardware encoding and software encoding techniques as

described in [14]. We set the constraints $[D_0, R_0]$ to $[60, 64]$ respectively indicating a good video quality of $30\,dB$ in $PSNR = 10\,log_{10}\frac{255^2}{D_0}$ and the achievable bit rate of the 3G wireless standard in $kbps$. Further setting a block length of $n = 222$ symbols for the RS coder with BPSK and QPSK modulations, we allow the H.263 video source coding variable T and channel coding variable k to assume values from the discrete sets $[2, 3, 5, 9, 12, 16, 25, 32]$ and $[40, , 50, 60, 70, 80, 90, 100, 112, 122, 132, 142, 152, 162] \cup [172, 182, 192, 202]$ respectively.

Despite the fact that our experimentation set up is fairly close to that of [14], we do not directly compare our results of utilizing the video source encoder of Section III.B with the results of [14]. This is because our model relies on the Gilbert-Elliott model rather than the Gilbert model of [14] and [18]. The Gilbert-Elliott model is a more general model than the Gilbert model associating non-trivial error probabilities to the GOOD and the BAD states. Furthermore, our model relates the average received signal to noise ratio to a Rayleigh distribution rather than the distance as reported in [14]. We believe that our model is more suitable for wireless channels due to the considerations of the fading effects. Instead, we compare the results of utilizing a single transmit antenna system with those of a double transmit antenna system in a Rayleigh fading channel under both Bernoulli and Gilbert-Elliot loss models. We also note that when the loss behavior of the channel is characterized by the Gilbert-Elliott model, we set $N_{0,G} = 0.1\,N_{0,B}$ to distinguish between the GOOD state and the BAD state. In the latter case, the constants $[\gamma, \beta]$ are set to $[0.99873, 0.875]$ indicating a burst length $L_B = \frac{1}{1-\beta} = 8$ as reported in [14].

Utilizing the Gauss-Markov source of Section III.A. with parameters $\rho = 0$ and $\rho = 0.9$ respectively, Fig. 3 through Fig. 6 plot the optimal values of P_{total}, the total power for the BPSK modulation scheme utilizing the hardware implementation technique versus the channel information symbol k or the average received signal to noise ratio $\overline{SNR}$ as defined in Equation (2). The results have been obtained for normalized values of ξ, σ^2_{gm}, $\mathcal{E}[|\alpha|^2]$, N_0, and a channel loss characterized by the Bernoulli model.

Fig. 7 through Fig. 10 plot similar curves for normalized values of ξ, σ^2_{gm}, $\mathcal{E}[|\alpha|^2]$, $N_{0,G}$, and a channel

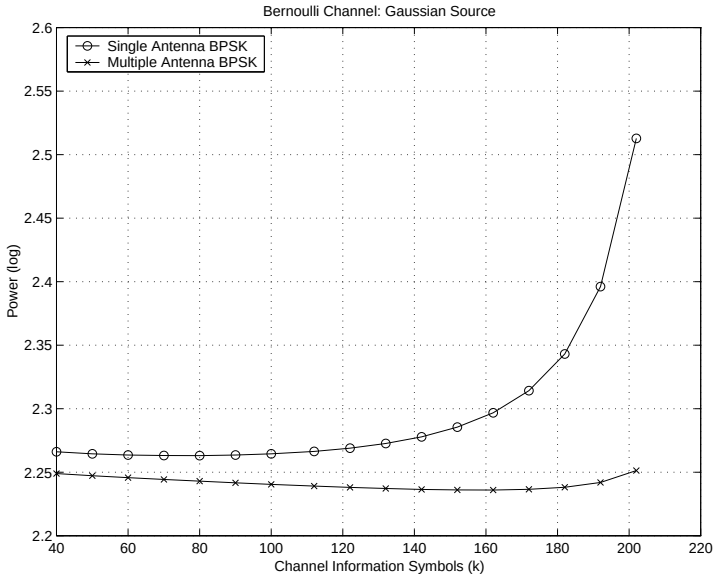

Fig. 3. BPSK plots of optimal power versus channel coding information symbols (k) for single and multiple transmit antenna systems utilizing hardware implementation. A memoryless Gaussian source ($\rho = 0$) has been utilized.

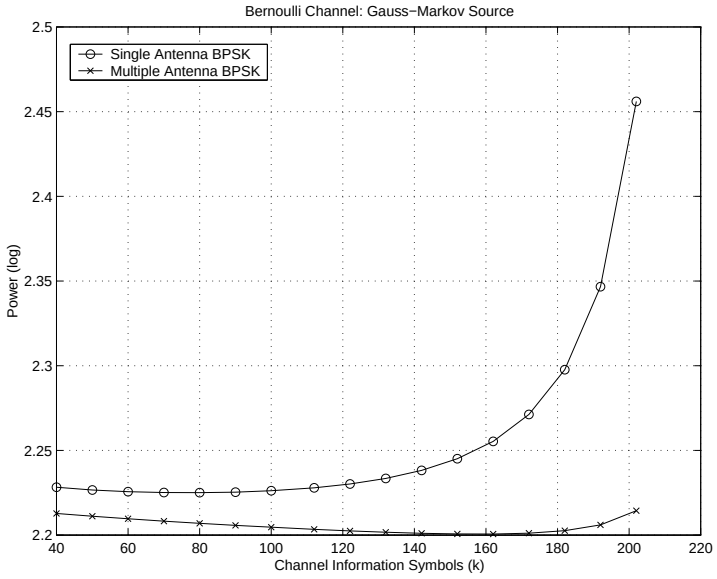

Fig. 4. BPSK plots of optimal power versus channel coding information symbols (k) for single and multiple transmit antenna systems utilizing hardware implementation. A Gauss-Markov source with parameter $\rho = 0.9$ has been utilized.

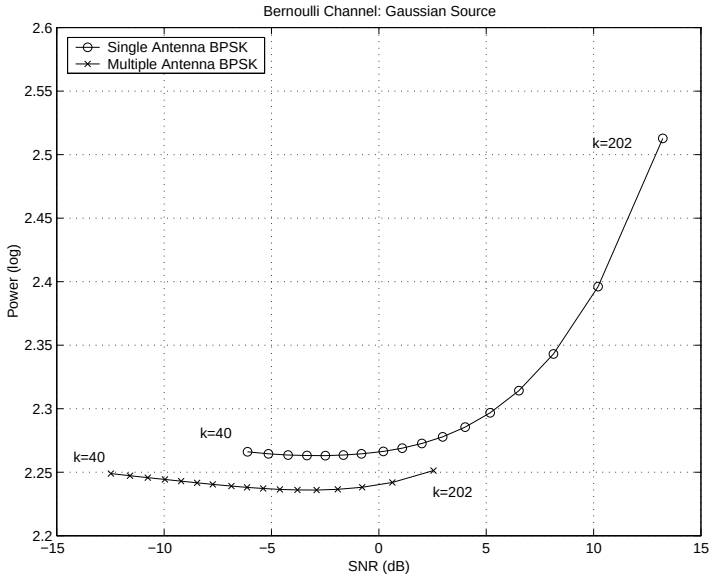

Fig. 5. BPSK plot of optimal power versus average received signal to noise ratio for single and multiple transmit antenna systems utilizing hardware implementation. A memoryless Gaussian source ($\rho = 0$) has been utilized.

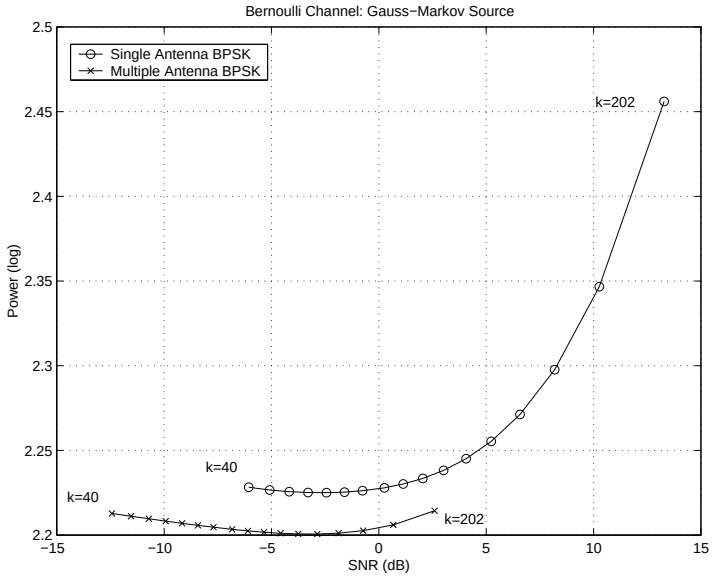

Fig. 6. BPSK plot of optimal power versus average received signal to noise ratio for single and multiple transmit antenna systems utilizing hardware implementation. A Gauss-Markov source with parameter $\rho = 0.9$ has been utilized.

loss characterized by the Gilbert-Elliott model.

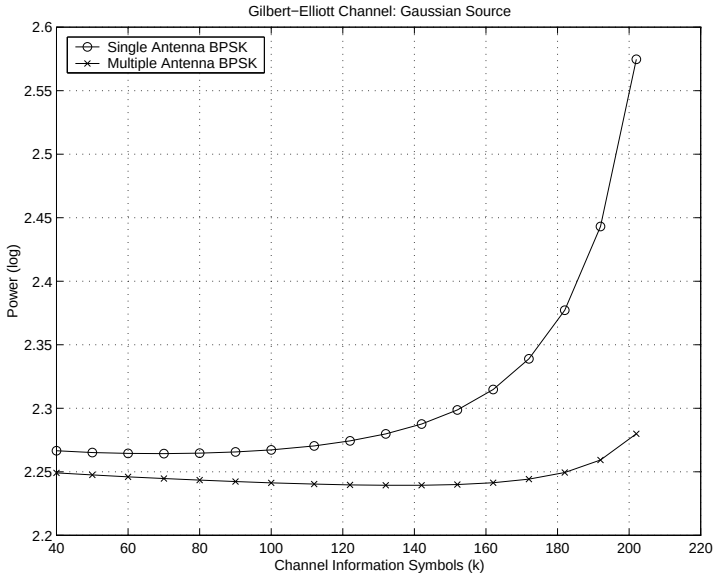

Fig. 7. BPSK plots of optimal power versus channel coding information symbols (k) for single and multiple transmit antenna systems utilizing hardware implementation. A memoryless Gaussian source ($\rho = 0$) has been utilized.

Fig. 15 and Fig. 14 plot the optimal values of P_{total}, the total power for the BPSK modulation scheme utilizing hardware and software implementation techniques versus the channel information symbol k or the average received signal to noise ratio $\overline{SNR}$. The results have been obtained for normalized values of σ_{u0}^2, $\mathcal{E}[|\alpha|^2]$, N_0, and a channel loss characterized by the Bernoulli model.

Fig. 15 and Fig. 18 plot similar curves for the QPSK modulation scheme.

Fig. 19 through Fig. 26 plot similar curves as those of Fig. 11 through Fig. 18 respectively for normalized values of ξ, σ_{gm}^2, $\mathcal{E}[|\alpha|^2]$, $N_{0,G}$, and a channel loss characterized by the Gilbert-Elliott model.

The most striking observation when comparing the figures is the fact that the optimal power of a multiple antenna system is consistently lower than that of a single antenna system across the range of average received signal to noise ratios. This is the case when employing the BPSK or the QPSK modulation, utilizing the Gauss-Markov source of Section III.A or the video source of Section III.B, and finally characterizing a channel loss behavior under the Bernoulli or the Gilbert-Elliott models.

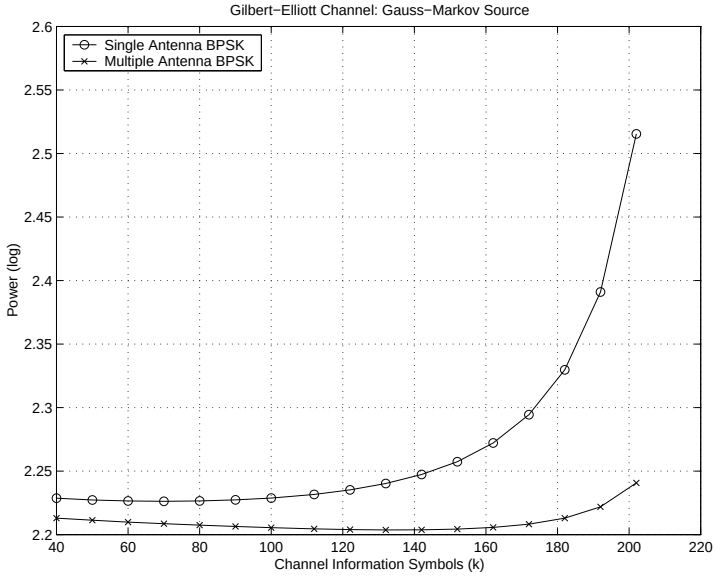

Fig. 8. BPSK plots of optimal power versus channel coding information symbols (k) for single and multiple transmit antenna systems utilizing hardware implementation. A Gauss-Markov source with parameter $\rho = 0.9$ has been utilized.

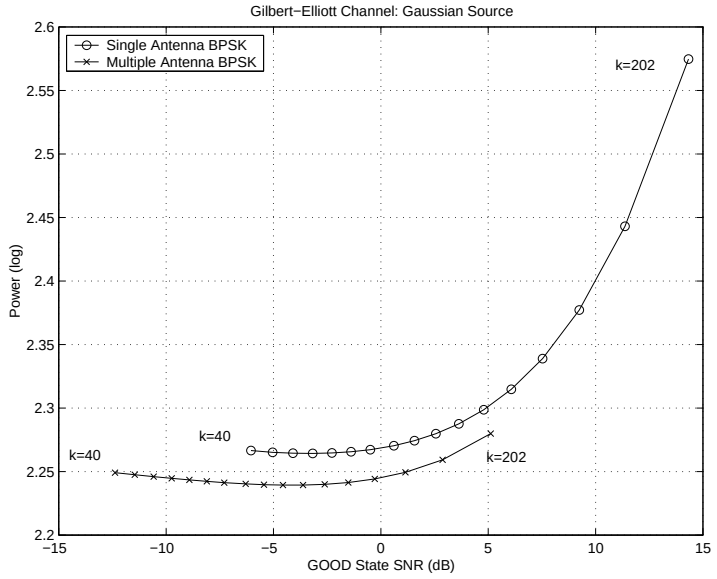

Fig. 9. BPSK plot of optimal power versus the GOOD state average received signal to noise ratio ($N_{0,G} = 0.1\, N_{0,B}$) for single and multiple transmit antenna systems utilizing hardware implementation. A memoryless Gaussian source ($\rho = 0$) has been utilized.

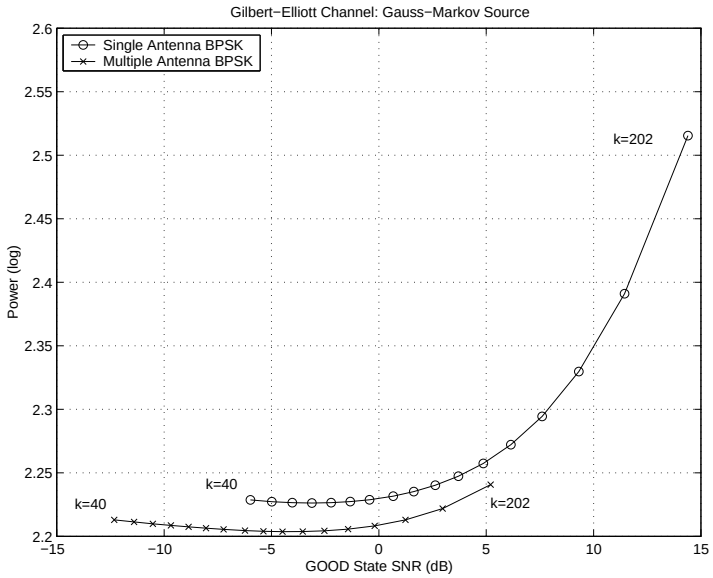

Fig. 10. BPSK plot of optimal power versus the GOOD state average received signal to noise ratio ($N_{0,G} = 0.1\, N_{0,B}$) for single and multiple transmit antenna systems utilizing hardware implementation. A Gauss-Markov source with parameter $\rho = 0.9$ has been utilized.

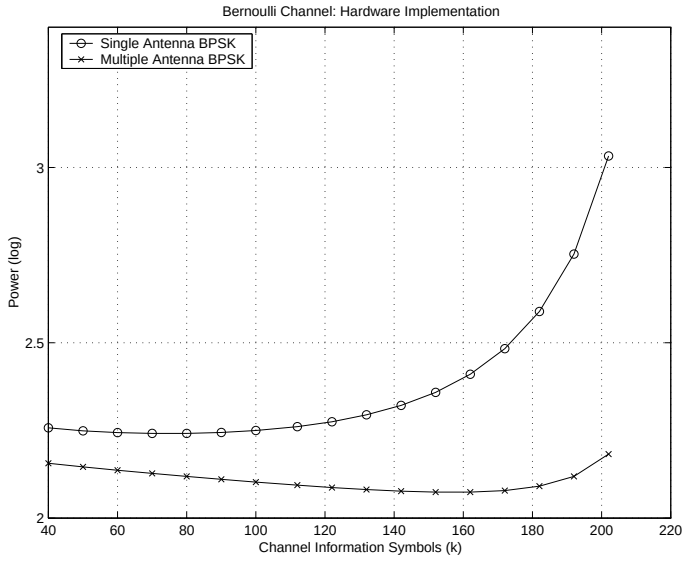

Fig. 11. BPSK plots of optimal power versus channel coding information symbols (k) for single and multiple transmit antenna systems utilizing hardware implementation. Containership.qcif video source has been utilized.

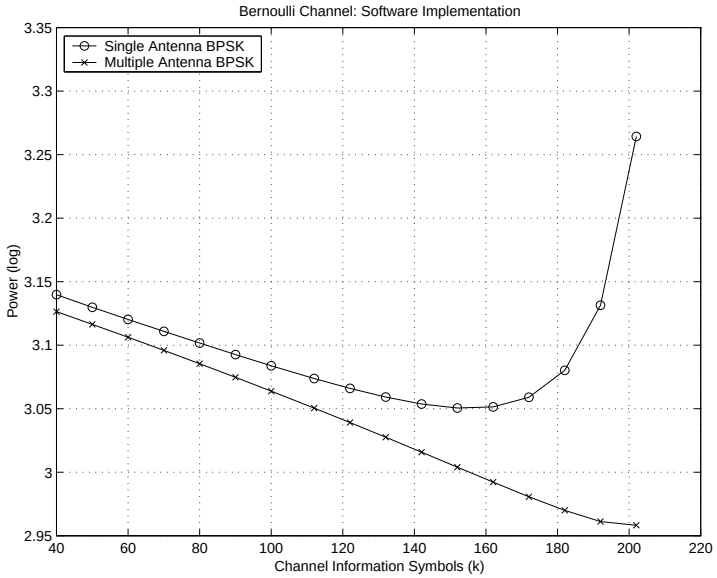

Fig. 12. BPSK plots of optimal power versus channel coding information symbols (k) for single and multiple transmit antenna systems utilizing software implementation. Containership.qcif video source has been utilized.

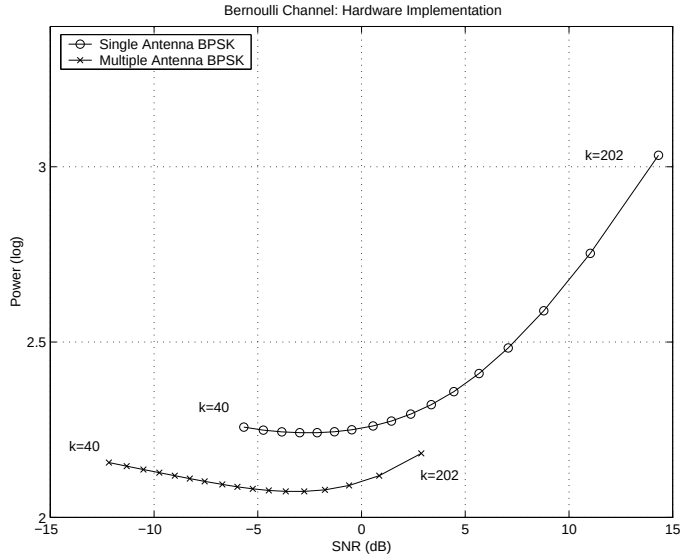

Fig. 13. BPSK plot of optimal power versus average received signal to noise ratio for single and multiple transmit antenna systems utilizing hardware implementation. Containership.qcif video source has been utilized.

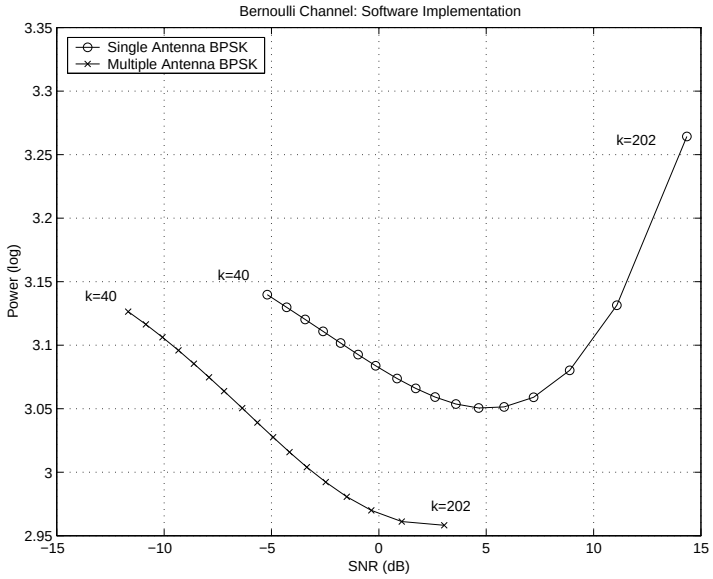

Fig. 14. BPSK plot of optimal power versus average received signal to noise ratio for single and multiple transmit antenna systems utilizing software implementation. Containership.qcif video source has been utilized.

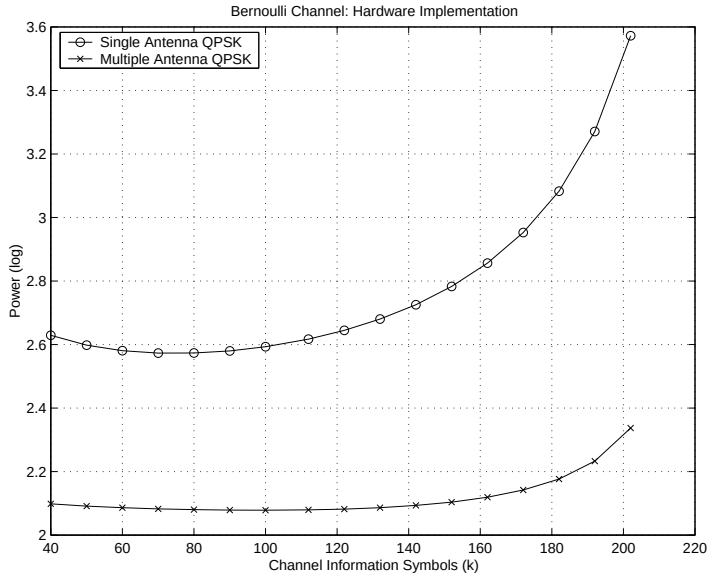

Fig. 15. QPSK plots of optimal power versus channel coding information symbols (k) for single and multiple transmit antenna systems utilizing hardware implementation. Containership.qcif video source has been utilized.

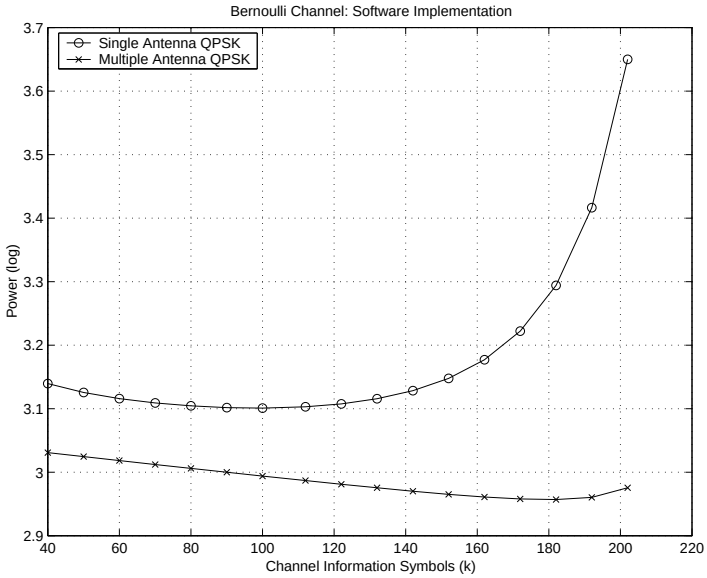

Fig. 16. QPSK plots of optimal power versus channel coding information symbols (k) for single and multiple transmit antenna systems utilizing software implementation. Containership.qcif video source has been utilized.

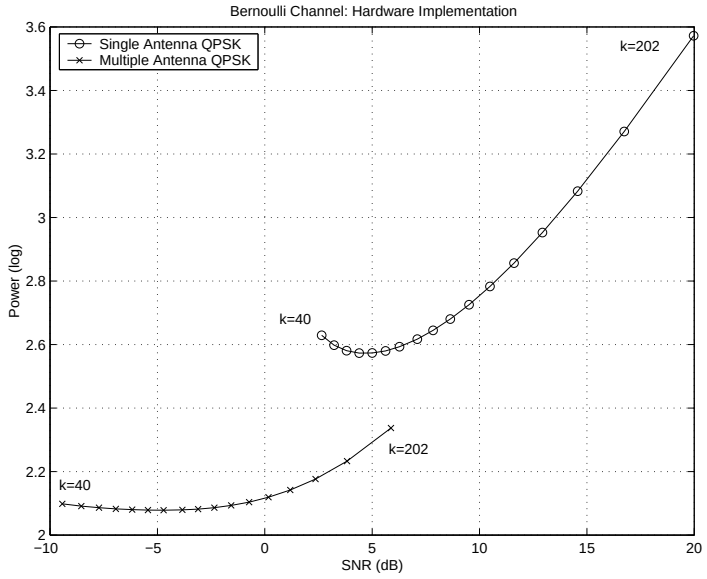

Fig. 17. QPSK plot of optimal power versus average received signal to noise ratio for single and multiple transmit antenna systems utilizing hardware implementation. Containership.qcif video source has been utilized.

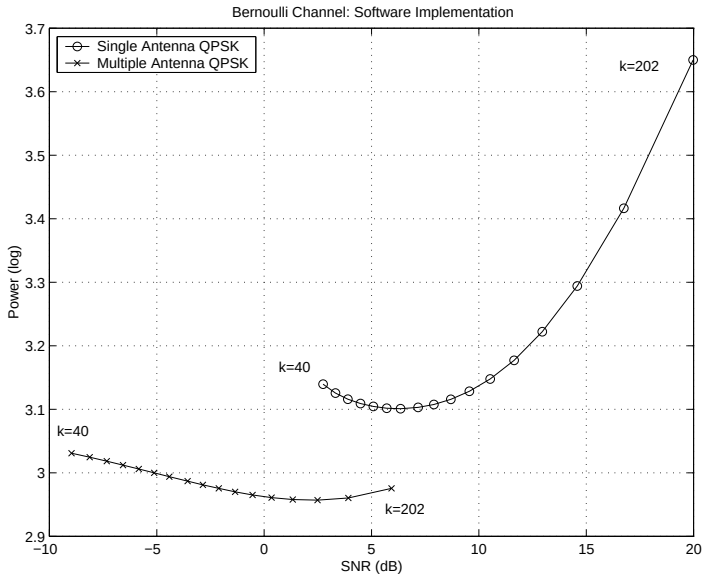

Fig. 18. QPSK plot of optimal power versus average received signal to noise ratio for single and multiple transmit antenna systems utilizing software implementation. Containership.qcif video source has been utilized.

We also note that the choice of scaling factors in our reported experiments for hardware and software implementations lead to similar qualitative behaviors.

It is also worth mentioning that we have conducted another set of experiments for a channel loss characterized by the Gilbert-Elliott model and a burst length of $L_B = \frac{1}{1-\beta} = 32$. Although not shown in the figures, our findings exhibit a similar qualitative behavior and are consistent with the reported results of this section. We refer the interested reader to [23] for further numerical results.

VI. Conclusions

In this paper, we presented a pair of solutions to the general problem of power control in wireless media systems with multiple transmit antennas. We provided an analysis of the underlying wireless system consisting of transmitting, channel, and receiving sides. Relying on our analysis results, we formulated an optimization problem aimed at minimizing the total power consumption of wireless media systems subject to a given quality of service level and an available bit rate. Our formulation considered the power

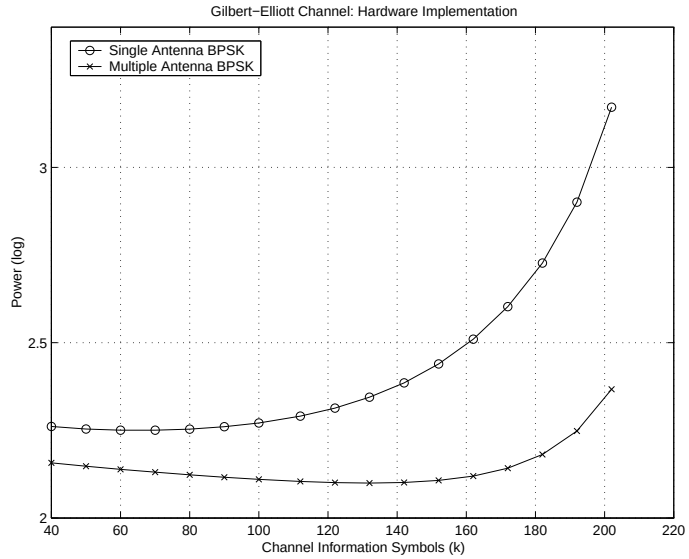

Fig. 19. BPSK plots of optimal power versus channel coding information symbols (k) for single and multiple transmit antenna systems utilizing hardware implementation. Containership.qcif video source has been utilized.

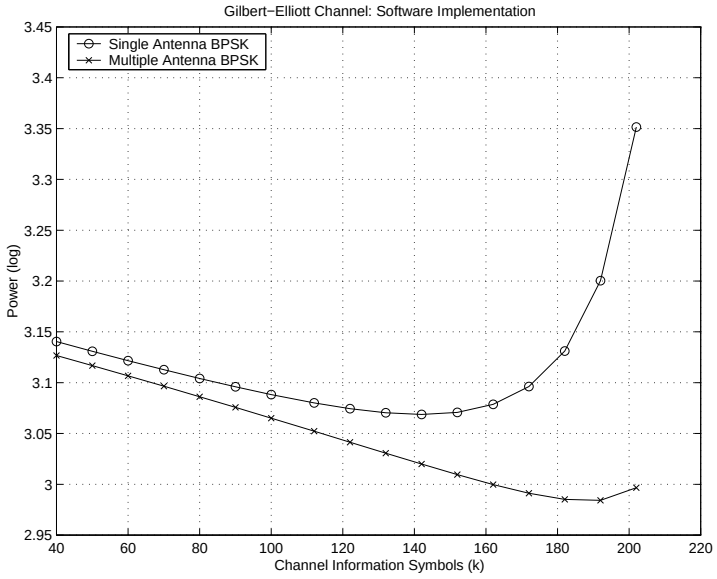

Fig. 20. BPSK plots of optimal power versus channel coding information symbols (k) for single and multiple transmit antenna systems utilizing software implementation. Containership.qcif video source has been utilized.

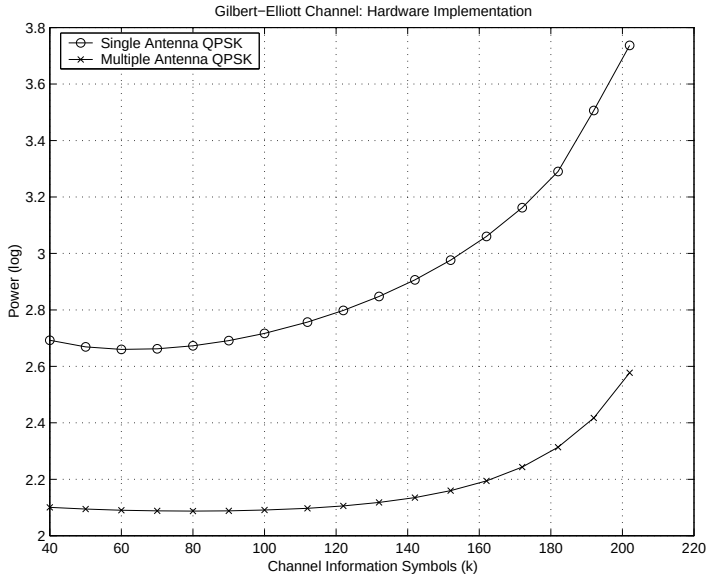

Fig. 21. QPSK plots of optimal power versus channel coding information symbols (k) for single and multiple transmit antenna systems utilizing hardware implementation. Containership.qcif video source has been utilized.

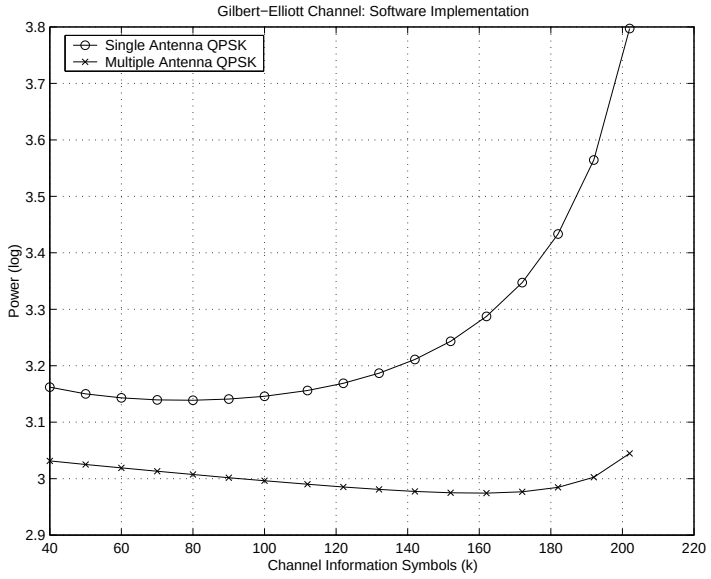

Fig. 22. QPSK plots of optimal power versus channel coding information symbols (k) for single and multiple transmit antenna systems utilizing software implementation. Containership.qcif video source has been utilized.

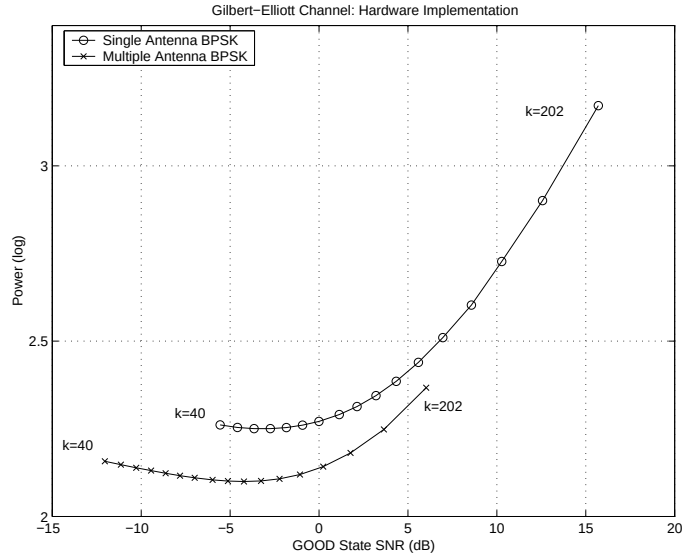

Fig. 23. BPSK plot of optimal power versus the GOOD state average received signal to noise ratio ($N_{0,G} = 0.1\, N_{0,B}$) for single and multiple transmit antenna systems utilizing hardware implementation. Containership.qcif video source has been utilized.

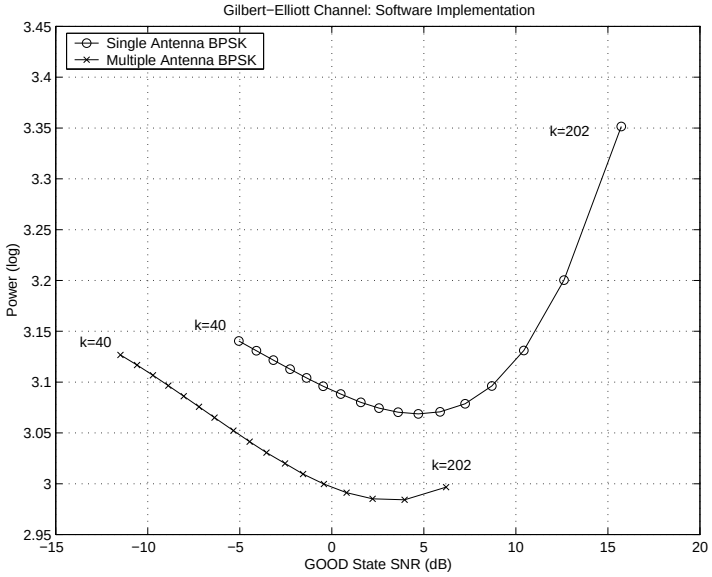

Fig. 24. BPSK plot of optimal power versus the GOOD state average received signal to noise ratio ($N_{0,G} = 0.1\, N_{0,B}$) for single and multiple transmit antenna systems utilizing software implementation. Containership.qcif video source has been utilized.

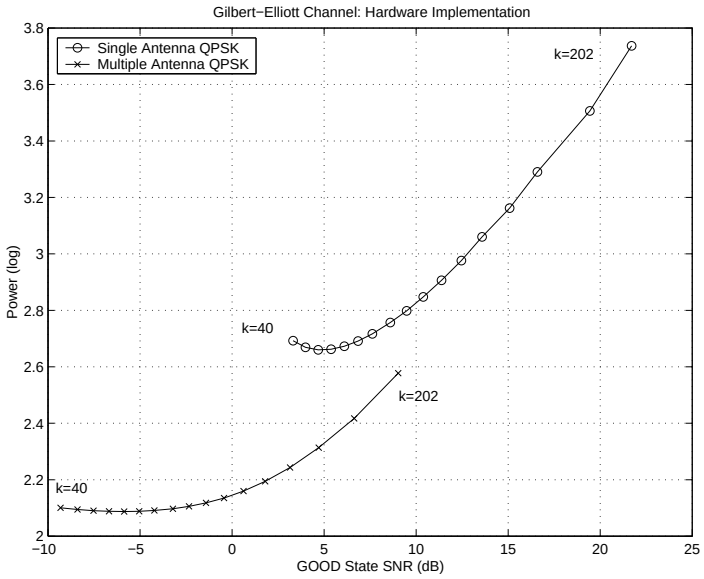

Fig. 25. QPSK plot of optimal power versus the GOOD state average received signal to noise ratio ($N_{0,G} = 0.1\, N_{0,B}$) for single and multiple transmit antenna systems utilizing hardware implementation. Containership.qcif video source has been utilized.

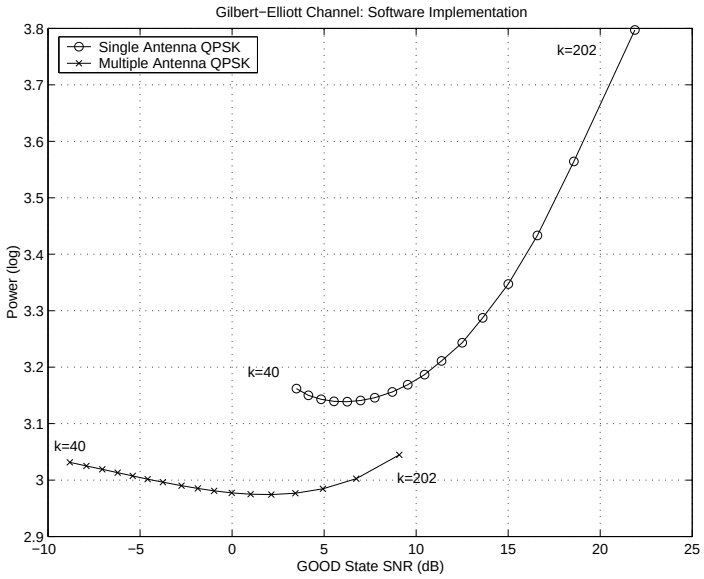

Fig. 26. QPSK plot of optimal power versus the GOOD state average received signal to noise ratio ($N_{0,G} = 0.1\, N_{0,B}$) for single and multiple transmit antenna systems utilizing software implementation. Containership.qcif video source has been utilized.

consumption related to source coding, channel coding, and transmission of multiple transmit antennas. While our source coding analysis utilized both a Gauss-Markov source and a video source, our channel coding analysis relied on Rayleigh fading channels along with the Bernoulli/Gilbert-Elliott loss models. Finally, our transmission analysis used space-time block codes. We evaluated the performance of our power optimized solution for both single and double transmit antenna systems and observed that the fact that our multiple transmit antenna system was consistently offering lower power consumptions. We are currently working on the expansion of our results into the layered and replicated media scenarios as a general combined framework for distributing multimedia content over the wireless backbone. We are focusing on both coding and networking aspects of the problem. In the networking side, we are relating our Layered Media Multicast Control (LMMC) research results of [21] and [22] to the present work. In addition, we are developing novel content processing algorithms capable of providing video summaries, thereby further reducing the power consumption of a wireless system.

REFERENCES

[1] S.M. Alamouti, "A Simple Transmitter Diversity Scheme for Wireless Communications," IEEE JSAC, November 1998.

[2] D.P. Bertsekas, "Nonlinear Programming, 2nd Edition," Athena Scientific Publishing, 1999.

[3] D.P. Bertsekas, "Dynamic Programming and Optimal Control, 2nd Edition," Athena Scientific Publishing, 1999.

[4] E.O. Elliott, "Estimates on Error Rates for Codes on Burst-Noise Channels," Bell Syst. Tech. J., vol. 42, pp. 1977-1997, September 1963.

[5] S. Appadwedula, M. Goel, N.R. Shanbhad, D.L. Jones, K. Ramchandran, "Total System Energy Minimization for Wireless Image Transmission," Journal of VLSI Signal Processing Systems, vol. 27, no. 1/2, pp. 99-117, February 2001.

[6] A. Gersho, R.M. Gray, "Vector Quantization and Signal Compression," Kluwer Academic Publishers, 1992.

[7] E.N. Gilbert, "Capacity of A Burst-Noise Channel," Bell Syst. Tech J., vol. 39, pp. 1253-1265, September 1960.

[8] M. Goel, S. Appadwedula, N.R. Shanbhag, K. Ramchandran, and D.L. Jones, "A Low-Power Multimedia Communication System for Indoor Wireless Applications," IEEE Workshop on SIPS99, 1999.

[9] P.J.M. Havinga, "Energy Efficiency of Error Correction on Wireless Systems," in Proc. of IEEE WCNC, September 1999.

[10] H. Jafarkhani, P. Ligdas, N. Farvardin, “Adaptive Rate Allocation in a Joint Source-Channel Coding Framework for Wireless Channels,” IEEE Vehicular Technology Conference (VTC-96), April 1996.

[11] Q. Zhang, W. Zhu, Z. Ji, Y-Q. Zhang, “A Power-Optimized Joint Source Channel Coding for Scalable Video Streaming over Wireless Channel,” in Proc. of IEEE ISCAS, 2001.

[12] Z. Ji, Q. Zhang, W. Zhu, Y-Q. Zhang, “End-to-end Power-Optimized Video Communication over Wireless Channels,” in Proc. of IEEE Workshop on MMSP, 2001.

[13] T. H. Lan and A. H. Tewfik, “Adaptive Low Power Multimedia Wireless Communications,” in Proc. of IEEE Workshop on MMSP, 1997.

[14] X. Lu, Y. Wang, E. Erkip, “Power Efficient H.263 Video Transmission over Wireless Channels,” in Proc. of IEEE ICIP, 2002.

[15] D.F. Shanno, “Conditioning of Quasi-Newton Methods for Function Minimization,” Mathematics of Computing, Vol. 24, pp 647-656, 1970.

[16] M.K. Simon, M.S. Alouini, “Digital Communication over Fading Channels: A Unified Approach to Performance Analysis,” John Wiley, ISBN: 0471317799, 2000.

[17] M.K. Simon, “Evaluation of Average Bit Error Probability for Space-Time Coding Based On a Simpler Exact Evaluation of Pairwise Error Probability,” Int’l Journal on Communications and Networks, September 2001.

[18] K. Stuhlmuller, N. Farber, M. Link and B. Girod, “Analysis of Video Transmission over Lossy Channels,” IEEE JSAC, June 2000.

[19] V. Tarokh, H. Jafarkhani, A.R. Calderbank, “Space-Time Block Coding from Orthogonal Designs,” IEEE Trans. Inform. Theory, July 1999.

[20] H. Yousefi’zadeh, H. Jafarkhani, “Analytical Modeling of Burst Loss: A Study of the Gilbert Model,” Submitted for Publication. Available at http://www.ece.uci.edu/˜hyousefi/pub.html.

[21] H. Yousefi’zadeh, H. Jafarkhani, A. Habibi “Layered Media Multicast Control (LMMC): Rate Allocation and Partitioning,” Submitted for Publication. Available at http://www.ece.uci.edu/˜hyousefi/pub.html.

[22] H. Yousefi’zadeh, H. Jafarkhani, A. Habibi “Layered Media Multicast Control (LMMC): Error Control,” Submitted for Publication. Available at http://www.ece.uci.edu/˜hyousefi/pub.html.

[23] H. Yousefi’zadeh, H. Jafarkhani, M. Moshfeghi, “Power Optimization of Wireless Media Systems with Space-Time Code Building Blocks,” CPCC Technical Report, Available at http://www.ece.uci.edu/˜hyousefi/pub.html.